IEEE Robotics and Automation Letters (RA-L) paper, presented at ICRA 2026, Vienna, Austria. Cite as RA-L paper.

Passive Multi-Task Compliance Control with Strict Priority through Energy Tanks

Erling Tveter[1], Bjørn Kåre Sæbø[1], Christian Ott[2], Kristin Y. Pettersen[1] and Jan Tommy Gravdahl[1]

***Abstract*— A robot with kinematical redundancy with respect to a main task may perform additional tasks simultaneously with the main one. Often, it is desirable to prioritize the performance of some tasks over that of others. To create a strict priority between the different tasks, meaning the performance of higher-prioritized tasks is unaffected by lower-prioritized tasks, null-space projections are often used. Null-space projections may, however, cause the closed-loop system to lose the desirable passivity property, which is necessary to ensure stable interactions with passive environments. In previous works, an energy tank has therefore been introduced to compensate for the potential activity stemming from the null-space projections. However, if the energy tank becomes empty when using these previous methods, the performance of the lower-prioritized tasks suffers more than when using a classical, non-passive hierarchical control scheme. Thus, a new approach to handling this case is proposed in this work. In the event of the energy tank becoming empty and unable to compensate for any null-space projection-induced activity, the hierarchy is ceded to preserve the passivity of the system, leading to better performance of the lower-prioritized tasks compared to previous passivation schemes. Output strict passivity of the closed-loop system is proven irrespective of the amount of energy available from the energy tank, and the performance of the proposed method is validated and compared to that of a classical hierarchical impedance controller and that of an earlier passivation method through simulation and experiments of redundant robotic manipulators.**

I. Introduction

When a robot goes in and out of physical contact with its environment, its dynamics will suddenly change. This may lead to the robot causing harm to itself and its environment as a result of the closed-loop system becoming unstable. It turns out that the closed-loop system being *passive* is a necessary condition for guaranteeing stable interactions with environments that are also passive: Any non-passive robot can be destabilized by a passive environment [1]. If the robot satisfies the stronger notion of *output strict* passivity as well, though, it no longer just satisfies a necessary condition for stability. Under certain conditions, it can then be shown to be finite-gain $\mathcal{L}_2$ stable too [2, Lem. 6.5]. Thus, passivity, and particularly output strict passivity, are desirable properties for any robot that might interact with its surroundings.

Another control approach that is often used when a robot manipulator may interact with its environment is impedance control [3]. During contact, this method typically yields better performance than simple position or force controllers do, as it commands a force based on the robot's position, velocity and acceleration, instead of just the error in either position or force. In this work, we will look at the special case where the desired inertia of the robot is its natural inertia, which eliminates the need for force feedback. This is called *compliance* control, and has proven to be an effective method for robot manipulators, including those that are *kinematically redundant* [4].

A kinematically redundant robot, meaning a robot with more actuated degrees of freedom (DoFs) than a task requires, can perform additional tasks simultaneously to the original task. Often, some of these tasks are more important to the user than others, and it is therefore desirable to prioritize some tasks' performance over that of others. Frameworks that allow such a prioritization of tasks are called *hierarchical* or *task-priority* control schemes [5]. These schemes are typically divided into two categories: *soft*, e.g. [6], and *strict* task priority, e.g. [7]. In strict task-priority schemes, the execution of higher-prioritized tasks is unaffected by that of any lower-prioritized tasks. If a soft task-priority scheme is used instead, the same guarantee cannot be given, and thus strict priority frameworks are often preferred. The strict task-priority frameworks may be implemented using optimization [8] or null-space projections [9], with the latter often being favoured due to typically being less computationally demanding. Thus, this is also the approach taken in this work.

It can be shown, however, that the use of null-space projections may lead to the closed-loop system losing the desirable passivity property [10]. The stability of robots with classical hierarchical controllers based on null-space projections can therefore not be guaranteed during physical contact with passive environments. To remedy this, [10] and [11] introduced a virtual energy tank to the system to compensate for the possible activity caused by the null-space projections.

Virtual energy tanks are virtual reservoirs of pre-stored energy that can be used to passivate actions that would otherwise be active. The concept has been used in for instance [12]–[14] to maintain the desired performance of tasks achieved by non-passive controllers, but, when an action would violate passivity using a classical controller, the virtual tank is drained of energy instead, such that the total energy of the system does not increase.

The work from [10] and [11] was extended in [15] and [16] to not only passivate null-space projections, but also a time-varying stiffness in the compliance controller. The latter of the two also placed an additional layer of safety on the system by bounding its kinetic energy from above. All of these methods, [10], [11], [15] and [16], suffer from the same drawback, though: When the energy tank is empty, the performance of all lower-priority tasks suffers even more

than what it would do if a standard non-passive hierarchical compliance controller was used.

In this work, the method presented in [11] is modified such that the above problem does not occur. The possible passivity-violations stemming from null-space projections are compensated for by using energy tanks, just as in the previously mentioned works. However, instead of further sacrificing the performance of lower-priority tasks if the energy tank becomes empty, the null-space projections are removed from the scheme. As a result, there is no longer a hierarchy between the tasks. The passivity of the system is still ensured, however, and, in contrast to previous methods, the originally lower-prioritized tasks' performance does not suffer as a result of the energy tank being completely drained. The proposed method is proven to ensure output strict passivity, yielding advantageous stability results in the input-output sense, and is validated through simulations of a fully actuated double pendulum and experiments using a Franka Emika Panda robot manipulator. The results of the simulations and experiments are then compared to those gotten from the classical hierarchical impedance controller and the method presented in [11].

It should be noted that, in the view of the authors, the proposed method is not an *improvement* of [11], but rather an *alternative* to it that has complementary properties. While [11] always preserves the strict task hierarchy, but yields steady-state errors in the lower-priority tasks if the energy tank is empty, the proposed method does not yield steady-state errors, but cedes the hierarchy if the tank is empty. Depending on the application, one approach might be preferred over the other, but it is not clear that either one is superior in general. If the performance of the main task is safety-critical, choosing the previous method is prudent, whereas if preserving steady-state accuracy of lower-priority tasks is important, while some degradation in transient performance of higher-priority tasks is acceptable, the proposed approach may be more suitable.

The paper is organized as follows: In Section II, the fundamentals of hierarchical control and a previous approach to passivate such a controller is presented. Then, in Section III, the proposed method is presented and proven to yield output strict passivity. The simulation and experimental results validating the method are given in Section IV, before the conclusions and future work are presented in Section V.

II. Background

The dynamics of an n-DoF robot manipulator with joint configuration given by $\boldsymbol{q} \in \mathbb{R}^n$ can be described by the following equation:

$$\boldsymbol{M}(\boldsymbol{q})\ddot{\boldsymbol{q}} + \boldsymbol{C}(\boldsymbol{q},\dot{\boldsymbol{q}})\dot{\boldsymbol{q}} + \boldsymbol{g}(\boldsymbol{q}) = \boldsymbol{\tau} + \boldsymbol{\tau}^{\text{ext}}. \tag{1}$$

Here, $\boldsymbol{M}(\boldsymbol{q}) = \boldsymbol{M}(\boldsymbol{q})^T > \boldsymbol{0} \in \mathbb{R}^{n\times n}$ is the inertia matrix, $\boldsymbol{C}(\boldsymbol{q},\dot{\boldsymbol{q}}) \in \mathbb{R}^{n\times n}$ is the Coriolis matrix and $\boldsymbol{g}(\boldsymbol{q}) \in \mathbb{R}^n$ is the generalized gravitational forces, while $\boldsymbol{\tau} \in \mathbb{R}^n$ and $\boldsymbol{\tau}^{\text{ext}} \in \mathbb{R}^n$ are the control input and the generalized external forces acting on the robot, respectively. The Coriolis matrix is formulated such that $\dot{\boldsymbol{M}}(\boldsymbol{q}) = \boldsymbol{C}(\boldsymbol{q},\dot{\boldsymbol{q}}) + \boldsymbol{C}(\boldsymbol{q},\dot{\boldsymbol{q}})^T$ holds. From this point on, we will omit the matrices' dependencies for the sake of readability when the dependencies are clear from the context or already defined.

A task hierarchy consisting of r tasks can be defined as follows: Each task coordinate is given by $\boldsymbol{x}_i = \boldsymbol{f}_i(\boldsymbol{q}) \in \mathbb{R}^{m_i}$, and its velocity by

$$\dot{\boldsymbol{x}}_i = \frac{\partial \boldsymbol{f}_i(\boldsymbol{q})}{\partial \boldsymbol{q}}\dot{\boldsymbol{q}} = \boldsymbol{J}_i(\boldsymbol{q})\dot{\boldsymbol{q}}, \tag{2}$$

where $i = 1,\dots,r$ and $m_i \in \mathbb{N}$. The tasks are ordered by their priority such that the highest prioritized task has index $i = 1$ and the lowest prioritized task has index $i = r$, and the sum of the task dimensions is assumed to be equal to the robot's number of DoFs, $\sum_{i=1}^{r} m_i = n$. Furthermore, each Jacobian $\boldsymbol{J}_i$ is assumed to be full row rank, and the stacked Jacobian, $\boldsymbol{J} = [\boldsymbol{J}_1^T,\dots,\boldsymbol{J}_r^T]^T$, is assumed to be non-singular. To be able to conclude output strict passivity instead of just passivity in Section III-C, we also assume that the smallest singular value of $\boldsymbol{J}$ is lower bounded away from zero:

$$\sigma_{\min}(\boldsymbol{J}) \geq \underline{\sigma} > 0. \tag{3}$$

This is the case if, for instance, $\boldsymbol{q}$ belongs to a compact space (and the previous assumption on $\boldsymbol{J}$ holds).

A. Hierarchical dynamics

To avoid lower-priority tasks from interfering with the execution of higher-prioritized tasks, a hierarchical controller can be used. To express the dynamic equation of the strict hierarchy, we first introduce the hierarchy-consistent task velocities $\boldsymbol{v}_i \in \mathbb{R}^{m_i}$ for $i = 1,\dots,r$:

$$\begin{bmatrix}\boldsymbol{v}_1\\ \vdots \\ \boldsymbol{v}_r\end{bmatrix} = \begin{bmatrix}\bar{\boldsymbol{J}}_1\\ \vdots \\ \bar{\boldsymbol{J}}_r\end{bmatrix}\dot{\boldsymbol{q}} = \bar{\boldsymbol{J}}\dot{\boldsymbol{q}}. \tag{4}$$

Here, the $\bar{\boldsymbol{J}}_i$ matrices, which will be defined in the next paragraph, are the dynamically consistent Jacobian matrices that make up the invertible matrix $\bar{\boldsymbol{J}} \in \mathbb{R}^{n\times n}$. By premultiplying by $\bar{\boldsymbol{J}}^{-T}$ and using (4), the dynamics (1) can be written as

$$\boldsymbol{\Lambda}(\boldsymbol{q})\dot{\boldsymbol{v}} + \boldsymbol{\mu}(\boldsymbol{q},\dot{\boldsymbol{q}})\boldsymbol{v} = \bar{\boldsymbol{J}}(\boldsymbol{q})^{-T}\left(-\boldsymbol{g}(\boldsymbol{q}) + \boldsymbol{\tau} + \boldsymbol{\tau}^{\text{ext}}\right), \tag{5}$$

where $\boldsymbol{\Lambda} = \bar{\boldsymbol{J}}^{-T}\boldsymbol{M}\bar{\boldsymbol{J}}^{-1} \in \mathbb{R}^{n\times n}$ is the block-diagonal inertia matrix, and $\boldsymbol{\mu} = \boldsymbol{\Lambda}\left(\bar{\boldsymbol{J}}\boldsymbol{M}^{-1}\boldsymbol{C} - \dot{\bar{\boldsymbol{J}}}\right)\bar{\boldsymbol{J}}^{-1} \in \mathbb{R}^{n\times n}$ is the Coriolis matrix that satisfies $\dot{\boldsymbol{\Lambda}} = \boldsymbol{\mu} + \boldsymbol{\mu}^T$.

Each dynamically consistent task Jacobian is described by $\bar{\boldsymbol{J}}_i = \left(\boldsymbol{Z}_i\boldsymbol{M}\boldsymbol{Z}_i^T\right)^{-1}\boldsymbol{Z}_i\boldsymbol{M} \in \mathbb{R}^{m_i\times n}$, apart from for the top-prioritized task, which is the same as the original task Jacobian, $\bar{\boldsymbol{J}}_1 = \boldsymbol{J}_1$. The $\boldsymbol{Z}_i$ matrices are null-space base matrices of the augmented Jacobian matrix $\boldsymbol{J}_{i-1}^{\text{aug}} = \left[\boldsymbol{J}_1^T,\dots,\boldsymbol{J}_{i-1}^T\right]^T$ fulfilling $\boldsymbol{J}_j\boldsymbol{Z}_k^T = \boldsymbol{0}\ \forall k > j$, and a full expression for them can be found in e.g. [7]. For consistency, we will denote $\boldsymbol{Z}_1 = \left(\boldsymbol{J}_1^{M+}\right)^T$, where $\boldsymbol{J}_1^{M+} = \boldsymbol{M}^{-1}\boldsymbol{J}_1^T(\boldsymbol{J}_1\boldsymbol{M}^{-1}\boldsymbol{J}_1^T)^{-1}$ is the dynamically consistent pseudoinverse [9].

For ease of notation, we will mainly use the classical null-space projector [9],

$$\boldsymbol{N}_i = (\boldsymbol{I} - (\boldsymbol{J}_{i-1}^{\text{aug}})^T((\boldsymbol{J}_{i-i}^{\text{aug}})^{M+})^T), \tag{6}$$

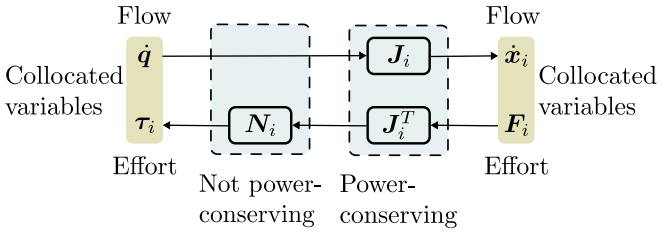

Fig. 1. Non-passive, classical hierarchical impedance control for task $i = 2, \dots, r$. In contrast to the transposed Jacobian $\boldsymbol{J}_i^T$, the null-space projector $\boldsymbol{N}_i$ does not have a dual counterpart in the flow-path. The total transformation is thus not power-conserving.

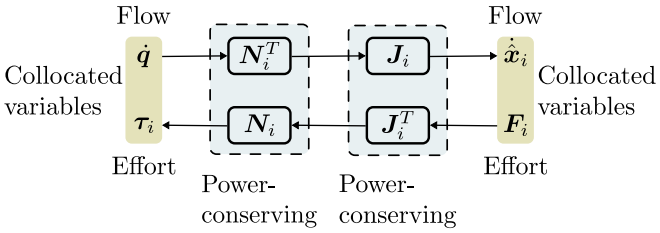

Fig. 2. Scheme from [10] and [11] for task $i = 2, \dots, r$ to maintain the passivity when the energy tank is empty. A dual counterpart to the null-space projector $\boldsymbol{N}_i$ is introduced in the flow-path, which maintains the passivity of the system, but alters the task velocity $\dot{\hat{\boldsymbol{x}}}_i$ apparent to the controller.

in this work instead of the null-space base matrix $\boldsymbol{Z}_i$. The two are related through

$$\boldsymbol{N}_i \boldsymbol{J}_i^T = \bar{\boldsymbol{J}}_i^T \boldsymbol{Z}_i \boldsymbol{J}_i^T, \tag{7}$$

and one can thus always use $\bar{\boldsymbol{J}}_i^T \boldsymbol{Z}_i$ instead of $\boldsymbol{N}_i$ in this work. Note that using $\boldsymbol{N}_i$ is for notational simplicity and that the use of $\boldsymbol{Z}_i$ is recommended in practice, as it is often less computationally expensive [17].

B. Classical non-passive hierarchical impedance control

The classical way of achieving impedance control in a strict task-priority framework is to design a control law of the form [7]

$$\boldsymbol{\tau} = \boldsymbol{g} + \boldsymbol{\tau}_\mu + \sum_{i=1}^{r} \boldsymbol{\tau}_i, \tag{8}$$

where $\boldsymbol{g}$ compensates for the gravitational forces, $\boldsymbol{\tau}_\mu$ compensates for the off-blockdiagonal terms of $\boldsymbol{\mu}$, decoupling the task dynamics, and $\boldsymbol{\tau}_i$ is the torque performing task i. By applying (8) to the dynamics (5), the closed-loop dynamics are then given in a hierarchically decoupled manner by

$$\boldsymbol{\Lambda} \dot{\boldsymbol{v}} + \mathrm{blkdiag}(\boldsymbol{\mu}) \boldsymbol{v} = \bar{\boldsymbol{J}}^{-T} \left(\sum_{i=1}^{r} \boldsymbol{\tau}_i + \boldsymbol{\tau}^{\mathrm{ext}} \right). \tag{9}$$

The task-related torques $\boldsymbol{\tau}_i$ are given by

$$\boldsymbol{\tau}_i = \boldsymbol{N}_i \boldsymbol{J}_i^T \boldsymbol{F}_i, \tag{10}$$

where the operational space force $\boldsymbol{F}_i$ is first transformed to a joint torque by $\boldsymbol{J}_i^T$, and then projected onto the null-space of the higher-prioritized tasks by $\boldsymbol{N}_i$. The force $\boldsymbol{F}_i$ is chosen as

$$\boldsymbol{F}_i(\boldsymbol{x}_i, \dot{\boldsymbol{x}}_i) = -\boldsymbol{K}_i \tilde{\boldsymbol{x}}_i - \boldsymbol{D}_i \dot{\boldsymbol{x}}_i \tag{11}$$

to realize the desired spring-damper behavior of the closed-loop system (9), (10). Here, $\tilde{\boldsymbol{x}}_i = \boldsymbol{x}_i - \boldsymbol{x}_{i,d}$ is the error of task i, as $\boldsymbol{x}_{i,d} \in \mathbb{R}^{m_i}$ is the constant desired task state, while $\boldsymbol{K}_i \in \mathbb{R}^{m_i \times m_i}$ and $\boldsymbol{D}_i \in \mathbb{R}^{m_i \times m_i}$ are positive definite stiffness and damping matrices, respectively.

This classical impedance controller does, however, not yield a passive system. As seen in Fig. 1, which is essentially the same as [10, Fig. 1], we cannot guarantee that the power $\dot{\boldsymbol{x}}_i^T \boldsymbol{F}_i$ is not increased through the transformation to the power $\dot{\boldsymbol{q}}^T \boldsymbol{\tau}_i$, meaning we cannot guarantee the passivity of the system. This is due to the null-space projector $\boldsymbol{N}_i$ not having a dual counterpart in the flow-path, which would render the transformation power-conserving.

C. Previous passivation approach

To restore the desired passivity of the system, [10] and [11] introduce an energy tank to the system. This virtual reservoir of energy is then used to compensate for any activity introduced by the null-space projections, leaving the system passive.

To not mask any potentially dangerous active behavior, the tank is usually not filled with large amounts of energy, meaning it can become empty. If this happens, the energy tank can no longer be used to passivate the system, and the tank and the controller are therefore designed such that passivity is preserved even if the tank is empty. However, this comes at a price.

As mentioned in Section II-B, the non-passivity of the classical hierarchical controller comes as a result of there not being a dual to the null-space projector $\boldsymbol{N}_i$ in the flow-path relating $\dot{\boldsymbol{q}}$ to $\dot{\boldsymbol{x}}$, so the dual is now introduced when the energy tank becomes empty, see Fig. 2. This maintains both the passivity and the strict hierarchy of the system, but alters the task velocity $\dot{\hat{\boldsymbol{x}}}_i$ apparent to the controller, such that the task force (11) is given by $\boldsymbol{F}_i(\hat{\boldsymbol{x}}_i, \dot{\hat{\boldsymbol{x}}}_i)$.

As the joint velocities can be found by $\dot{\boldsymbol{q}} = \sum_{j=1}^{r} \boldsymbol{Z}_j^T \boldsymbol{v}_j$ [7], the task velocities can be expressed as [11]

$$\dot{\boldsymbol{x}}_i = \underbrace{\boldsymbol{J}_i \sum_{j=1}^{i-1} \boldsymbol{Z}_j^T \boldsymbol{v}_j}_{\boldsymbol{w}_i} + \underbrace{\boldsymbol{J}_i \boldsymbol{Z}_i^T \boldsymbol{v}_i}_{\boldsymbol{\kappa}_i}, \tag{12}$$

by using (2) and the property $\boldsymbol{J}_i \boldsymbol{Z}_j^T = \boldsymbol{0}\ \forall j > i$. Here, $\boldsymbol{w}_i$ is the component of the task velocity stemming from higher-prioritized tasks' motions, while $\boldsymbol{\kappa}_i$ is the component stemming from the current task level. The introduction of $\boldsymbol{N}_i^T$ in the flow-path cancels out $\boldsymbol{w}_i$, and the task velocity apparent to the controller, $\dot{\hat{\boldsymbol{x}}}_i$, can thus be written as

$$\dot{\hat{\boldsymbol{x}}}_i = \begin{cases} \boldsymbol{w}_i + \boldsymbol{\kappa}_i + \boldsymbol{K}_{P,i}(\boldsymbol{x}_i - \hat{\boldsymbol{x}}_i) & E_t \geq \underline{E}_t \\ \boldsymbol{\kappa}_i & \text{else.} \end{cases} \tag{13}$$

Here, E_t is the energy in the energy tank, $\underline{E}_t$ is the lower limit of the energy tank and $\boldsymbol{K}_{P,i}(\boldsymbol{x}_i - \hat{\boldsymbol{x}}_i)$ is a drift compensation term. Thus, when the tank is empty, the controller will no longer yield a control input based on the full task

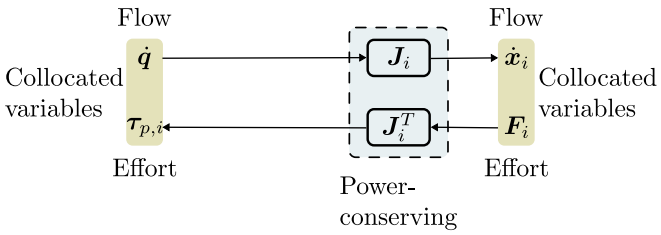

Fig. 3. Proposed scheme for task $i = 2, \dots, r$ to maintain the passivity when the energy tank is empty. To preserve the passivity, the null-space projector $\boldsymbol{N}_i$ is removed, meaning that the task hierarchy is abandoned. In contrast to the scheme from [10] and [11], though, the task velocity $\dot{\boldsymbol{x}}_i$ remains unaltered.

velocity $\dot{\boldsymbol{x}}_i$, but based only on the part stemming from the task itself, $\boldsymbol{\kappa}_i$.

The task available to the controller, $\hat{\boldsymbol{x}}_i$, is found through numerically integrating $\dot{\hat{\boldsymbol{x}}}_i$. Therefore, modifying the velocity signal leads to drift in $\boldsymbol{x}_i$. This means that, contrary to the classical hierarchical impedance controller (8), (10) and (11), the previous passivation approach [11] may yield a steady-state error if the energy tank becomes empty, even if all the tasks are compatible.

III. Approach

To avoid the problems introduced by the scheme presented in [10] and [11], the proposed approach involves preserving the passivity through ceding the strict task hierarchy when the energy tank is empty. Instead of modifying the flow, we modify the effort signal, i.e. we modify the force instead of the velocity, see Fig. 3. Thus, the controller has access to the true task states and velocities, and the drift causing the steady-state errors is therefore eliminated.

In this section we will first present the proposed control law and the energy tank design, before the (output strict) passivity of the closed-loop system will be proven.

A. Control law

The control law is also here chosen to be of the form (8). In this work, however, we split each task-related part of the control input, $\boldsymbol{\tau}_i$, into a passive and potentially non-passive part:

$$\boldsymbol{\tau} = \boldsymbol{g} + \boldsymbol{\tau}_\mu + \sum_{i=1}^{r} \boldsymbol{\tau}_i \tag{14a}$$

$$\boldsymbol{\tau}_i = \boldsymbol{\tau}_{p,i} + \boldsymbol{\tau}_{np,i} \tag{14b}$$

$$\boldsymbol{\tau}_{p,i} = \boldsymbol{J}_i^T \boldsymbol{F}_i \tag{14c}$$

$$\boldsymbol{\tau}_{np,i} = \alpha(\boldsymbol{N}_i - \boldsymbol{I})\boldsymbol{J}_i^T \boldsymbol{F}_i. \tag{14d}$$

Here, $\boldsymbol{\tau}_{p,i}$ is the non-null-space-projected part of the control input that ensures passivity even without the use of an energy tank, as shown in Fig. 3. The second summand, $\boldsymbol{\tau}_{np,i}$, on the other hand, does not ensure passivity on its own, and therefore includes a valve parameter, α, which determines if the controller can use the energy from the energy tank. When the valve parameter $\alpha = 1$, $\boldsymbol{\tau}_{np,i}$ cancels $\boldsymbol{\tau}_{p,i}$ and replaces it with the null-space projected control input from the classical hierarchical impedance controller (10). When $\alpha = 0$, on the other hand, $\boldsymbol{\tau}_i = \boldsymbol{\tau}_{p,i}$, which means that the strict hierarchy is lost, but the passivity is ensured.

The valve parameter α is defined with a smooth transition between zero and one as in [13] to avoid a discontinuous control law that could cause unnecessary wear on the robot due to sudden changes in the commanded acceleration:

$$\alpha = \begin{cases} 0 & E_t \leq \underline{E}_t \\ \frac{1}{2}\left(1 - \cos\left(\frac{E_t - \underline{E}_t}{\delta_\alpha}\pi\right)\right) & \underline{E}_t < E_t < \underline{E}_t + \delta_\alpha \\ 1 & \text{otherwise.} \end{cases} \tag{15}$$

Here, $E_t \in \mathbb{R}$ is the energy in the tank, $\underline{E}_t > 0$ its lower limit, and $\delta_\alpha \geq 0$ a parameter controlling the smoothness of the valve transition. The valve ensures that only the passive, non-projected component, $\boldsymbol{\tau}_{p,i}$, is applied when the tank is depleted and can no longer compensate for potential passivity violations from $\boldsymbol{\tau}_i$.

A smaller δ_α causes the controller to behave like the classical controller (8), (10) and (11) for a longer time, assuming the initial tank energy $E_{t,0} > \underline{E}_t$. The same holds for a larger $E_{t,0}$. The initial energy is typically set as the *task energy* E_T, which is the estimated minimum energy to achieve the task, plus the tank minimum, $E_{t,0} = E_T + \underline{E}_t$ [12]. The trade-off for choosing a small δ_α is a more abrupt switching, potentially causing large changes in the commanded acceleration.

Note that, similar to [11] and [13], one can also apply a different valve parameter α_i for each task. These parameters are dependent on the power that each specific task drains from the tank, such that a task may be executed as desired even if the energy tank is empty, given that the specific task in question does not require energy from the tank to preserve passivity. This is recommended in practice, as it may yield increased performance, but is not included here to better highlight the differences between the different methods during the simulations and experiments in Section IV.

B. Energy tank design

We design the energy tank such that the dynamics of the tank is given by

$$\dot{E}_t = \gamma \sum_{i=1}^{r} \left(\beta_i \dot{\boldsymbol{x}}_i^T \boldsymbol{D}_i \dot{\boldsymbol{x}}_i - \dot{\boldsymbol{q}}^T \boldsymbol{\tau}_{np,i}\right), \tag{16}$$

where

$$\gamma = \begin{cases} 0 & E_t \geq \bar{E}_t \cap \sum_{i=1}^{r} (\beta_i \dot{\boldsymbol{x}}_i^T \boldsymbol{D}_i \dot{\boldsymbol{x}}_i - \dot{\boldsymbol{q}}^T \boldsymbol{\tau}_{np,i}) > 0 \\ 1 & \text{otherwise,} \end{cases} \tag{17}$$

is the overflow valve from [11], rewritten for a single energy tank. This valve makes sure that the energy level of the tank does not exceed some predetermined maximum level $\bar{E}_t > 0$. The user-specified $\beta_i \in [0, 1)$ is a damping refill coefficient determining how much of the energy dissipated by the control effort for task i is used to refill the energy tank. The energy E_t in the tank is given by [1]

$$E_t = \frac{1}{2} s^2, \tag{18}$$

meaning that $\dot{E}_t = s\dot{s}$. The tank state s does not represent a physical quantity, but is merely a measure of the tank energy, with dynamics that can be chosen as part of the control design. To get the desired tank dynamics (16), we therefore choose $\dot{s}$ accordingly:

$$\dot{s} = \frac{\gamma}{s}\sum_{i=1}^{r}\left(\beta_i \dot{\boldsymbol{x}}_i^T \boldsymbol{D}_i \dot{\boldsymbol{x}}_i - \dot{\boldsymbol{q}}^T \boldsymbol{\tau}_{np,i}\right), \tag{19}$$

and achieve the desired energy tank dynamics (16). Note that division by the tank state s is not a problem, as the state is bounded from below by $\sqrt{2\underline{E}_t} > 0$ through the valve (15). This is the reason that the tank's energy is lower-bounded by $\underline{E}_t > 0$.

C. Passivity analysis

In this subsection, we will provide a proof of the output strict passivity of the closed-loop system, (5), (14), (19), with respect to the input $\boldsymbol{\tau}^{\text{ext}}$ and the output $\dot{\boldsymbol{q}}$, and thus also its finite-gain $\mathcal{L}_2$ stability. As in [11], the passivity analysis will consist of two major steps. In the first step, a storage function related to the closed-loop system's potential energy is used, before the system's total internal energy is considered in the second step.

We first define a potential energy-like storage function for the closed-loop system

$$S_{\text{pot}} = \frac{1}{2}\sum_{i=1}^{r}\tilde{\boldsymbol{x}}_i^T \boldsymbol{K}_i \tilde{\boldsymbol{x}}_i + E_t \tag{20}$$

and its time derivative

$$\dot{S}_{\text{pot}} = \sum_{i=1}^{r}\dot{\boldsymbol{x}}_i^T \boldsymbol{K}_i \tilde{\boldsymbol{x}}_i + \dot{E}_t. \tag{21}$$

An alternative expression for $\dot{\boldsymbol{x}}_i^T \boldsymbol{K}_i \tilde{\boldsymbol{x}}_i$ is then found, relating it to $\dot{\boldsymbol{q}}^T \boldsymbol{\tau}_i$. We start by finding an alternative expression for $\dot{\boldsymbol{q}}^T \boldsymbol{\tau}_{np,i}$:

$$\begin{aligned}\dot{\boldsymbol{q}}^T \boldsymbol{\tau}_{np,i} &= \alpha \dot{\boldsymbol{q}}^T (\boldsymbol{N}_i - \boldsymbol{I}) \boldsymbol{J}_i^T \boldsymbol{F}_i \\ &= \alpha \boldsymbol{v}_i^T \boldsymbol{Z}_i \boldsymbol{J}_i^T \boldsymbol{F}_i - \alpha \dot{\boldsymbol{x}}_i^T \boldsymbol{F}_i \\ &= -\alpha \boldsymbol{w}_i^T \boldsymbol{F}_i,\end{aligned} \tag{22}$$

where (2), (4), (7) and (12) have been used. Using this relation, (22), along with (2), (14b) and (14c), we find an expression for $\dot{\boldsymbol{q}}^T \boldsymbol{\tau}_i$:

$$\begin{aligned}\dot{\boldsymbol{q}}^T \boldsymbol{\tau}_i &= \dot{\boldsymbol{q}}^T \boldsymbol{\tau}_{p,i} + \dot{\boldsymbol{q}}^T \boldsymbol{\tau}_{np,i} \\ &= \dot{\boldsymbol{x}}_i^T \boldsymbol{F}_i - \alpha \boldsymbol{w}_i^T \boldsymbol{F}_i.\end{aligned} \tag{23}$$

Then, the alternative expression for $\dot{\boldsymbol{x}}_i^T \boldsymbol{K}_i \tilde{\boldsymbol{x}}_i$ can finally be found through (11) and (23):

$$\dot{\boldsymbol{x}}_i^T \boldsymbol{K}_i \tilde{\boldsymbol{x}}_i = -\dot{\boldsymbol{q}}^T \boldsymbol{\tau}_i - \dot{\boldsymbol{x}}_i^T \boldsymbol{D}_i \dot{\boldsymbol{x}}_i - \alpha \boldsymbol{w}_i^T \boldsymbol{F}_i. \tag{24}$$

We can then show output strict passivity of (5), (14), (19), with respect to $(\dot{\boldsymbol{q}}, -\sum_{i=1}^{r}\boldsymbol{\tau}_i)$ using S_{pot} as a storage function by extending (21), and using (2), (3), (16), (22) and (24):

$$\begin{aligned}\dot{S}_{\text{pot}} &= \sum_{i=1}^{r}\dot{\boldsymbol{x}}_i^T \boldsymbol{K}_i \tilde{\boldsymbol{x}}_i + \dot{E}_t \\ &= \sum_{i=1}^{r}(-\dot{\boldsymbol{q}}^T \boldsymbol{\tau}_i - \dot{\boldsymbol{x}}_i^T \boldsymbol{D}_i \dot{\boldsymbol{x}}_i - \alpha \boldsymbol{w}_i^T \boldsymbol{F}_i) \\ &\qquad + \gamma \sum_{i=1}^{r}\left(\beta_i \dot{\boldsymbol{x}}_i^T \boldsymbol{D}_i \dot{\boldsymbol{x}}_i - \dot{\boldsymbol{q}}^T \boldsymbol{\tau}_{np,i}\right) \\ &= \sum_{i=1}^{r}\left(-\dot{\boldsymbol{q}}^T \boldsymbol{\tau}_i - (1-\beta_i)\dot{\boldsymbol{x}}_i^T \boldsymbol{D}_i \dot{\boldsymbol{x}}_i\right) \\ &\qquad - (1-\gamma)\sum_{i=1}^{r}\left(\beta_i \dot{\boldsymbol{x}}_i^T \boldsymbol{D}_i \dot{\boldsymbol{x}}_i + \alpha \boldsymbol{w}_i^T \boldsymbol{F}_i\right) \\ &\leq -\dot{\boldsymbol{q}}^T \sum_{i=1}^{r}\boldsymbol{\tau}_i - \sum_{i=1}^{r}(1-\beta_i)\dot{\boldsymbol{x}}_i^T \boldsymbol{D}_i \dot{\boldsymbol{x}}_i \\ &\leq -\dot{\boldsymbol{q}}^T \sum_{i=1}^{r}\boldsymbol{\tau}_i - \dot{\boldsymbol{q}}^T \underbrace{\underline{\sigma}^2 \lambda_{\min}(\boldsymbol{D}_{1-\beta})\dot{\boldsymbol{q}}}_{\boldsymbol{\rho}(\dot{\boldsymbol{q}})},\end{aligned} \tag{25}$$

where $\boldsymbol{D}_{1-\beta} := \text{blkdiag}\left((1-\beta_i)\boldsymbol{D}_i\right)$ and $\lambda_{\min}(\boldsymbol{D}_{1-\beta})$ is its lowest eigenvalue. Here, $\dot{\boldsymbol{q}}^T \boldsymbol{\rho}(\dot{\boldsymbol{q}}) > 0 \ \forall \dot{\boldsymbol{q}} \neq \boldsymbol{0}$, due to $\beta_i \in [0, 1)$ and $\boldsymbol{D}_i > 0 \ \forall i$, and $\underline{\sigma} \neq 0$, see (3). Note that the first inequality of (25) holds, as we in (17) defined γ such that $\gamma = 0 \implies \sum_{i=1}^{r}(\beta_i \dot{\boldsymbol{x}}_i^T \boldsymbol{D}_i \dot{\boldsymbol{x}}_i + \alpha \boldsymbol{w}_i^T \boldsymbol{F}_i) > 0$. The second inequality holds as well, because $\lambda_{\min}(\boldsymbol{A})\boldsymbol{a}^T\boldsymbol{a} \leq \boldsymbol{a}^T\boldsymbol{A}\boldsymbol{a}$ for positive semi-definite matrices $\boldsymbol{A} = \boldsymbol{A}^T$.

Using a full internal energy-like storage function, we will now show the desired passivity property of the closed-loop system, given by (5) subject to the control input (14) and the energy tank state dynamics (19), with respect to $(\dot{\boldsymbol{q}}, \boldsymbol{\tau}^{\text{ext}})$. We first define the storage function

$$S = S_{\text{pot}} + \frac{1}{2}\boldsymbol{v}^T \boldsymbol{\Lambda} \boldsymbol{v}. \tag{26}$$

Then, by using the hierarchical dynamics (5), along with (4), (25) and that $\dot{\boldsymbol{\Lambda}} = \boldsymbol{\mu} + \boldsymbol{\mu}^T$, we can show that the time derivative of (26) has the desired relation to $\dot{\boldsymbol{q}}^T \boldsymbol{\tau}^{\text{ext}}$:

$$\begin{aligned}\dot{S} &= \dot{S}_{\text{pot}} + \frac{1}{2}\boldsymbol{v}^T \dot{\boldsymbol{\Lambda}} \boldsymbol{v} + \boldsymbol{v}^T \boldsymbol{\Lambda} \dot{\boldsymbol{v}} \\ &= \dot{S}_{\text{pot}} + \dot{\boldsymbol{q}}^T \sum_{i=1}^{r}\boldsymbol{\tau}_i + \dot{\boldsymbol{q}}^T \boldsymbol{\tau}^{\text{ext}} \\ &\leq -\dot{\boldsymbol{q}}^T \sum_{i=1}^{r}\boldsymbol{\tau}_i + \dot{\boldsymbol{q}}^T \sum_{i=1}^{r}\boldsymbol{\tau}_i + \dot{\boldsymbol{q}}^T \boldsymbol{\tau}^{\text{ext}} - \dot{\boldsymbol{q}}^T \boldsymbol{\rho}(\dot{\boldsymbol{q}}) \\ &= \dot{\boldsymbol{q}}^T \boldsymbol{\tau}^{\text{ext}} - \dot{\boldsymbol{q}}^T \boldsymbol{\rho}(\dot{\boldsymbol{q}}).\end{aligned} \tag{27}$$

The analysis can summarized in the following theorem and lemma:

Theorem 1: The closed-loop system (5), (14), (19) is output strictly passive with respect to $(\dot{\boldsymbol{q}}, \boldsymbol{\tau}^{\text{ext}})$.

Lemma 1: The closed-loop system, (5), (14), (19), with input $\boldsymbol{\tau}^{\text{ext}}$ and output $\dot{\boldsymbol{q}}$, is finite-gain $\mathcal{L}_2$ stable with an $\mathcal{L}_2$ gain less than or equal to $1/(\underline{\sigma}^2 \lambda_{\min}(\boldsymbol{D}_{1-\beta}))$.

Note that Lemma 1 follows directly from Theorem 1 and (27) using [2, Lem. 6.5].

IV. Simulations and Experiments

To validate the proposed method and show its differences to the classical hierarchical controller, (8), (10) and (11), and a previous passivation scheme [11], both a simulation and an experimental study were conducted. The task errors and the value of the storage function (26) were monitored to verify that the passivity of the closed-loop systems was kept at all times. To highlight the differences between the methods, the damping refill coefficients of (16) were set to $\beta_i = 0 \ \forall i = 1, \dots, r$, such that no refilling of the energy tank was allowed.

A. Simulations

For the simulations[4], a fully actuated double pendulum was used, with a hierarchy consisting of two position tasks, x_1 and x_2, at its end: one along the horizontal axis and one along the horizontal axis rotated $45°$ in the two-dimensional space, so that there is a clear coupling between the two tasks. The simulations were conducted in Matlab/Simulink using an ode3 solver with a fixed time step of 0.001 s. The controller gains are given in Table I, with $\boldsymbol{K}_{P,i}$ from (13) set to 10 Hz for the previous passivation approach. The initial energy level of the energy tank, $E_{t,0}$, was set to 15 J, and its lower limit $\underline{E_t}$ to 1 J to showcase the behavior of the system both with and without energy left in the energy tank. The parameter δ_α of (15) that decides the smoothing layer was set to the small value of 0.003 J to observe the change in the system's behavior once the tank is depleted more easily.

As expected when using the proposed method, the performance of the main task, x_1, suffers in comparison to the other two methods during the transient phase after the energy tank becomes empty, as illustrated in Fig. 4. Note, however, that there is virtually no steady-state error for either task using the proposed method. This contrasts with the significant steady-state error yielded by the previous passivation method [11] for the second task in the hierarchy. In fact, both the proposed method and the classical method achieve both tasks in the steady-state case, whereas the previous passivation method [11] only does so for the top-priority task, see Figs. 4 and 5. As shown in Section II, though, the classical method does not guarantee passivity, and as seen in Fig. 6, this causes the value of (26) to increase using this method, something that does not occur using the two other methods.

While this is a relatively simple example, it can still help illustrate the trade-offs between the methods; one can imagine a scenario where the steady-state error in the secondary task, x_2, leads the system to settle in a suboptimal configuration, requiring more energy to counteract gravity or causing increased wear on the joints. Whether the trade-off between a more desirable steady-state configuration for the lower-priority tasks and a less favorable transient response in the higher-priority task, x_1, is acceptable, will naturally depend on the specific application.

[4] https://turlab.itk.ntnu.no/turlab/snakegroup/nullspace-passivation

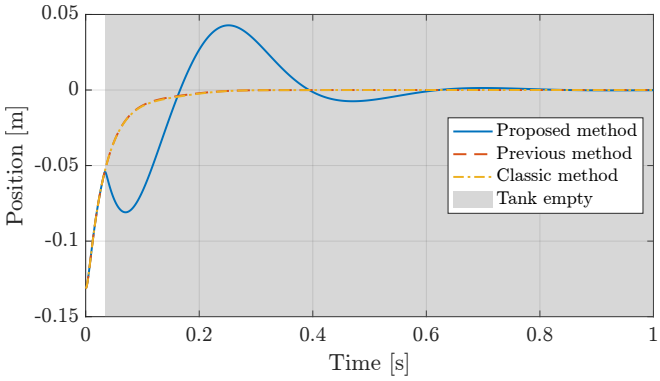

Fig. 4. Error $\tilde{\boldsymbol{x}}_1$ of the top-prioritized task using the three different control schemes during the simulations.

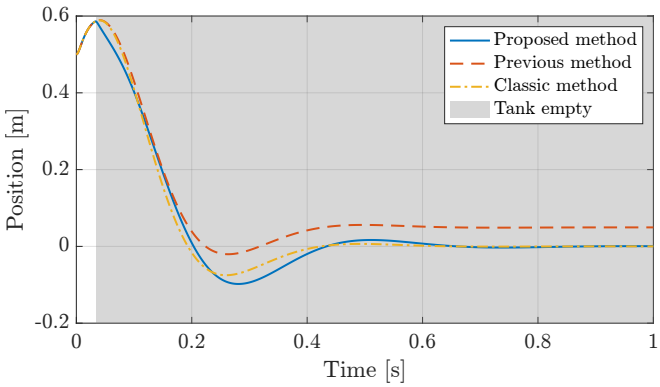

Fig. 5. Error $\tilde{\boldsymbol{x}}_2$ of the null-space task using the three different control schemes during the simulations.

TABLE I
The controller gains used in the simulations and the experiments.

	$\boldsymbol{K}_1$	$\boldsymbol{K}_2$	$\boldsymbol{K}_3$	$\boldsymbol{K}_4$	$\boldsymbol{D}_1$	$\boldsymbol{D}_2$	$\boldsymbol{D}_3$	$\boldsymbol{D}_4$
Sim.	750	200	-	-	$\sqrt{\boldsymbol{K}_1}$	$\sqrt{\boldsymbol{K}_2}$	-	-
Exp.	$300\boldsymbol{I}$	100	$100\boldsymbol{I}$	100	$2\sqrt{\boldsymbol{K}_1}$	20	$10\boldsymbol{I}$	5

B. Experiments

To further validate the method, experiments were conducted on a 7 DoF Franka Emika Panda robot manipulator, programmed using the Matlab/Simulink control interface, version 3.1. The tasks were chosen similarly to those in the simulations conducted in Section IV-A, except with more tasks to fully utilize the 7 DoFs available on the manipulator.

The highest priority task, $\boldsymbol{x}_1$ was the end-effector x- and y-positions in a frame equal to the base frame, but rotated $45°$ about the y-axis. The secondary task, x_2, was the end-effector z-position, $\boldsymbol{x}_3$ was the end-effector orientation and the fourth and final task, x_4 was the angle of the first joint of the robot. The task coordinates are visualized along with the robot in its initial configuration in Fig. 7. The gains used for the controllers are given in Table I, while all $\boldsymbol{K}_{P,i}$ from (13) used for the previous passivation approach were set to $3\boldsymbol{I}$ Hz. In order to allow precise regulation, while avoiding large system velocities during transients, each element of the proportional part of the task forces $\boldsymbol{F}_1$ and $\boldsymbol{F}_2$ from (11) were

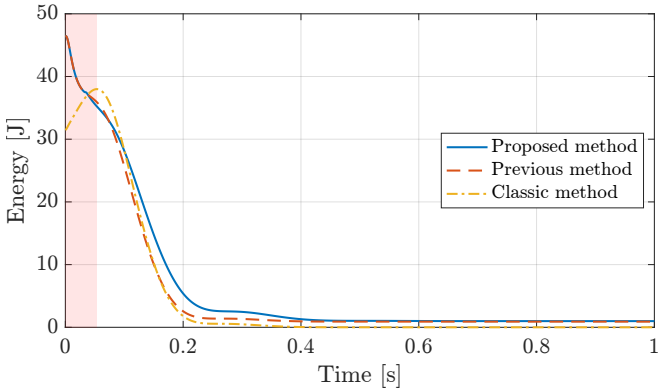

Fig. 6. Value of the storage function (26) for the proposed approach, the previous passivation approach [11], and the classical hierarchical impedance control scheme during the simulations. Note that the energy of the classical method increases in the red shaded region, and that the energies of the proposed and previous method do not converge to 0 due to $\underline{E}_t = 1$ J.

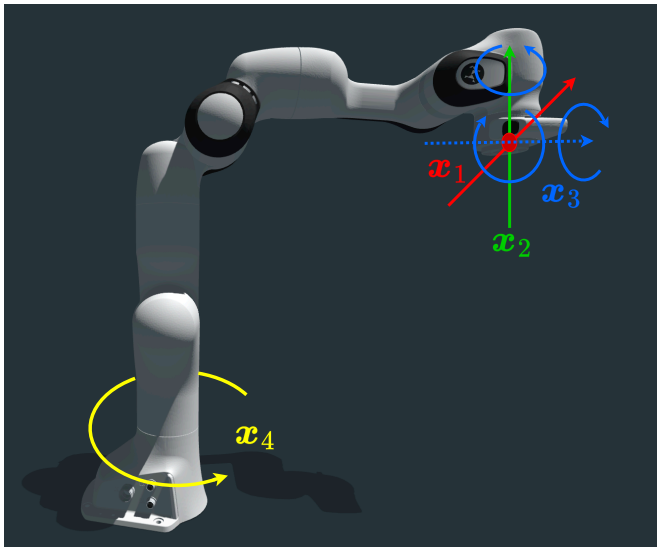

Fig. 7. The robot manipulator in its initial configuration with task coordinates.

saturated at 15 N, while the elements of the proportional part of $\boldsymbol{F}_3$ and $\boldsymbol{F}_4$ were saturated at 10 Nm. The parameter δ_α from (15) determining the smoothing layer between the two modes, energy in the tank and no energy in the tank, was set to 0.05 J, which is significantly larger than in the simulations. This was done to avoid violating any acceleration limits on the robot and unnecessary wear that a sudden change in commanded acceleration might cause. The initial tank energy was set to $E_{t,0} = 1.8$ J, and the lower energy tank limit to $\underline{E}_t = 1$ J such that both modes could be observed.

The robot was initialized at rest in the configuration that satisfied all tasks, with its joints at an initial angle of $\boldsymbol{q}_0 = \begin{bmatrix} 0 & 0 & 0 & -\pi/2 & 0 & \pi/2 & \pi/4 \end{bmatrix}^T$, see Fig. 7. Then, after two seconds, the setpoints of $\boldsymbol{x}_1$ and x_2 were moved in order to observe the transient behavior of the robot. The setpoints were moved relative to their initial values: 10 cm backwards in the rotated x-direction for $\boldsymbol{x}_1$ and 5 cm upwards in the z-direction for x_2. The setpoints of the remaining tasks were kept to their original values.

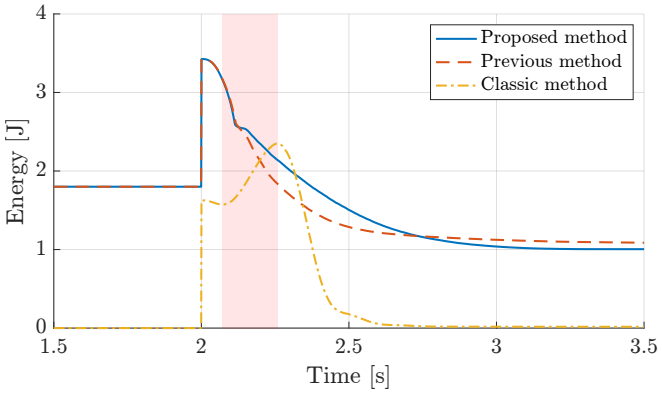

Fig. 8. Value of the storage function (26) for the proposed approach, the previous passivation approach [11], and the classical hierarchical impedance control scheme during the experiments. Note that the energy of the classical method increases in the red shaded region, and that the energies of the proposed and previous method do not converge to 0 due to $\underline{E}_t = 1$ J.

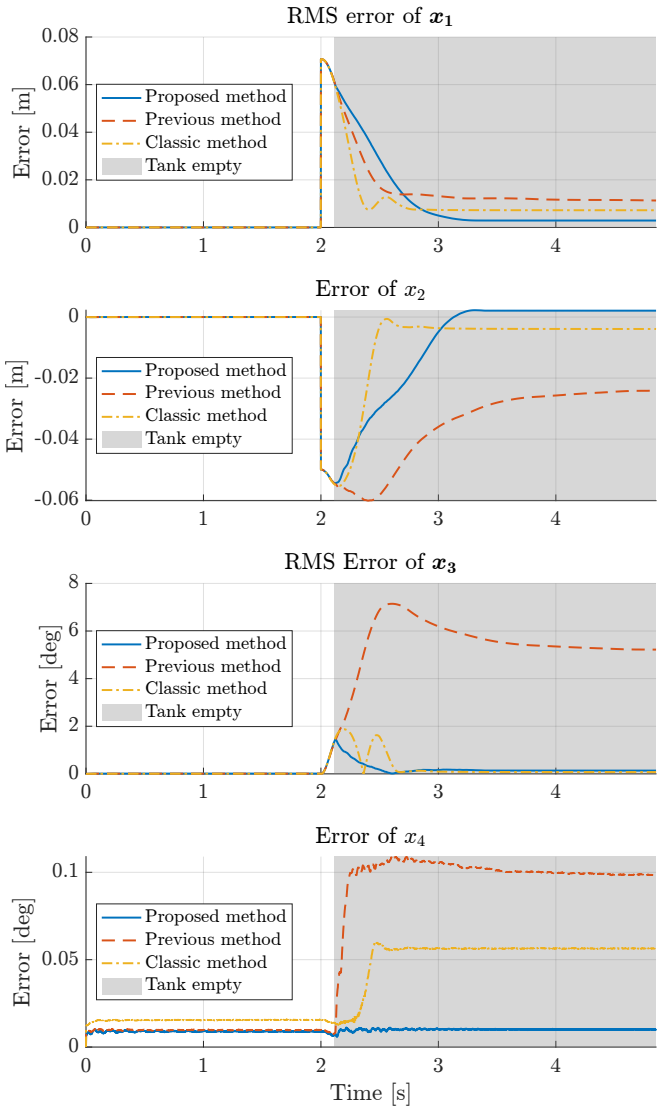

Fig. 9. Errors of all the tasks using the three different methods during the experiments.

Due to the rotation of the highest priority task's x-axis, there is a clear coupling between that and the second task x_2, as the task coordinates are not orthogonal to each other. While the initial and final configuration are fully compatible, the coupling effect can be seen during the transient.

In Fig. 8, the total energy in the system using the three different control approaches is shown. The energies were computed after the joint velocities had been smoothened through a moving average method to remove noise from the measurements. These smoothened joint velocities were only used in the computation of the energies, not in the controller. Note that the classical approach has no energy tank and thus no initial energy, in contrast to the two passivity-based approaches. Similarly, the total energy of the two passivity-based approaches converges to the minimum tank energy $\underline{E}_t$, while the energy of the classical method converges to 0 J. After two seconds, there is an initial increase in the energy of all three methods when the task set points are changed. One can clearly see that the classical approach continues to increase the energy in the system due to the competing tasks, while in the two other approaches the energy only decreases, even after the energy tanks have been depleted.

Comparing the performance of the controllers in Fig. 9, the performance of the main task $\boldsymbol{x}_1$ is quite equivalent for all controllers. The proposed controller has a slightly longer transient than the others, but also yields a slightly lower steady-state error. It should be noted that both the classical and proposed approaches theoretically should give zero steady-state error. However, as can be seen in the plots, perfect regulation is not achieved. This is due to unmodelled physical effects such as friction in the joints which cannot be compensated for by a proportional controller with no integral term. In the lower-prioritized tasks, however, the previous passivation approach yields noticeably worse performance than the two other methods do. This is especially noticeable in $\boldsymbol{x}_3$. Here, the previous passivation approach yields an average steady-state error of more than 4.5 degrees even though the tasks are kinematically compatible, while the two other methods yield virtually no steady-state error.

V. Conclusions

In this paper, we have proposed an energy tank scheme for output strictly passivating a strict hierarchical compliance controller, thus ensuring the $\mathcal{L}_2$ stability of the closed-loop system with respect to generalized external forces and joint velocities. In contrast to earlier passivation methods, the steady-state accuracy of the lower-priority tasks does not decrease further once the energy tank is empty. This is the result of the passivity being maintained by allowing all tasks to have the same priority once the energy tank is empty, instead of further deteriorating the performance of the lower-priority tasks. The proposed method has been proven to yield an output strictly passive system, and has been validated through both simulations and experiments. Furthermore, its merits have been showcased by comparing the results yielded by the proposed method to those yielded by a classical non-passive hierarchical impedance controller and a previously proposed passivation method. Through these comparisons, it is clear that the proposed method achieves better overall steady-state results than the previous passivation method, at the expense of worse behavior in the transients, particularly for the originally higher-prioritized tasks.

In future work, more complex sets of tasks for higher-dimensional systems such as humanoids or vehicle-manipulator systems could further verify the proposed method. Further comparison of the method with other passivity-based redundancy resolution schemes could also be interesting, for example comparing the proposed method to optimization-based methods.

Acknowledgments

We would like to thank Ph.D. students Jan Inge Dyrhaug and Simon A. Hoff, along with postdocs Erlend A. Basso and Henrik M. Schmidt-Didlaukies for their helpful suggestions and advice.

References

[1] S. Stramigioli, "Energy-Aware Robotics," in *Mathematical Control Theory I*, ser. Lecture Notes in Control and Information Sciences, M. K. Camlibel, A. A. Julius, R. Pasumarthy, and J. M. Scherpen, Eds. Springer International Publishing, 2015.

[2] H. Khalil, *Nonlinear Systems*, 3rd ed., ser. Pearson Education. Prentice Hall, 2002.

[3] N. Hogan, "Impedance Control: An Approach to Manipulation," in *Proc. American Control Conference*, 1984.

[4] A. Albu-Schaffer, C. Ott, U. Frese, and G. Hirzinger, "Cartesian impedance control of redundant robots: Recent results with the DLR-light-weight-arms," in *Proc. IEEE International Conference on Robotics and Automation*, vol. 3, 2003.

[5] Y. Nakamura, H. Hanafusa, and T. Yoshikawa, "Task-Priority Based Redundancy Control of Robot Manipulators," *The International Journal of Robotics Research*, vol. 6, no. 2, 1987.

[6] J. Salini, V. Padois, and P. Bidaud, "Synthesis of complex humanoid whole-body behavior: A focus on sequencing and tasks transitions," in *Proc. 2011 IEEE Int. Conf. on Robotics and Automation*, 2011.

[7] C. Ott, A. Dietrich, and A. Albu-Schäeffer, "Prioritized Multi-Task Compliance Control of Redundant Manipulators," *Automatica*, vol. 53, 2015.

[8] O. Kanoun, F. Lamiraux, and P.-B. Wieber, "Kinematic Control of Redundant Manipulators: Generalizing the Task-Priority Framework to Inequality Task," *IEEE Trans. on Robotics*, vol. 27, no. 4, 2011.

[9] O. Khatib, "A unified approach for motion and force control of robot manipulators: The operational space formulation," *IEEE Journal on Robotics and Automation*, vol. 3, no. 1, 1987.

[10] A. Dietrich, C. Ott, and S. Stramigioli, "Passivation of Projection-Based Null Space Compliance Control Via Energy Tanks," *IEEE Robotics and Automation Letters*, vol. 1, no. 1, 2016.

[11] A. Dietrich, X. Wu, K. Bussmann, C. Ott, A. Albu-Schäffer, and S. Stramigioli, "Passive Hierarchical Impedance Control Via Energy Tanks," *IEEE Robotics and Automation Letters*, vol. 2, no. 2, 2017.

[12] C. Schindlbeck and S. Haddadin, "Unified passivity-based Cartesian force/impedance control for rigid and flexible joint robots via task-energy tanks," in *Proc. IEEE International Conference on Robotics and Automation*, 2015.

[13] E. Shahriari, L. Johannsmeier, and S. Haddadin, "Valve-based Virtual Energy Tanks: A Framework to Simultaneously Passify Controls and Embed Control Objectives," in *Proc. American Control Conf.*, 2018.

[14] F. Benzi, M. Brunner, M. Tognon, C. Secchi, and R. Siegwart, "Adaptive Tank-based Control for Aerial Physical Interaction with Uncertain Dynamic Environments Using Energy-Task Estimation," *IEEE Robotics and Automation Letters*, vol. 7, no. 4, 2022.

[15] Y. Michel, C. Ott, and D. Lee, "Passivity-based variable impedance control for redundant manipulators," *IFAC-PapersOnLine*, vol. 53, no. 2, 2020.

[16] ——, "Safety-Aware Hierarchical Passivity-Based Variable Compliance Control for Redundant Manipulators," *IEEE Transactions on Robotics*, vol. 38, no. 6, 2022.

[17] C. Ott, *Cartesian Impedance Control of Redundant and Flexible-Joint Robots*. Berlin, Heidelberg: Springer Verlag, 2008, vol. 49.